Available online at www.sciencedirect.com
ScienceDirect
Trans. Nonferrous Met. Soc. China 26(2016) 1403−1409
Transactions of Nonferrous Metals Society of China
www.tnmsc.cn

Pore structure and liquid flow velocity distribution in water-saturated porous media probed by MRI

Ai-xiang WU[1,2], Chao LIU[1,2], Sheng-hua YIN[1,2], Zhen-lin XUE[1,2], Xun CHEN[1,2]

1. Key Laboratory of the Ministry of Education of China for High-Efficient Mining and Safety of Metal Mines, University of Science and Technology Beijing, Beijing 100083, China;
2. School of Civil and Environment Engineering, University of Science and Technology Beijing, Beijing 100083, China

Received 28 June 2015; accepted 6 January 2016

Abstract: Magnetic resonance imaging (MRI) was used to probe the structure and flow velocity within the interparticle space of a packed bed of agar beads under water-saturated condition. The images of the velocity field at three different flow rates were obtained. To determine the pore-parameter of the porous media, the internal structure of the bed was also obtained using image processing technique. The results show that the porosity of the sample is 31.28% and the fitting curve for the distribution of pore equivalent diameter follows Gaussian distribution. The velocity profiles do shift as the flow rate varies and the solution flow through the void space is not a homogeneous flow in any pores. The velocity distributions within the pore are roughly parabolic with the local maximum being near the center. About half of the velocity components are in the class of 0−1 cm/s. The frequency of lower velocity components is lower at higher flow rate, but to higher velocity components, it is just the opposite.

Key words: magnetic resonance imaging; porous media; flow velocity; porosity; pore equivalent diameter

1 Introduction

Pore structure of porous media, solution seepage and mass transfer processes within the void space are of fundamental importance to the leaching system [1]. It is generally known that the complexity of pore structure is the main reason for the complexities of solution distribution in granular media. Experimental and theoretical studies of pore structure and solution flow often treat porous media as an effectively homogeneous system. Such a method neglects the complexities of medium, although the details of flow distribution may be extremely crucial to the leaching system.

Restricted by technique, means and method, the traditional research on the seepage law of leaching solution usually treated the leaching dump as a black box. A slice of basic principles and applications of soil mechanics, hydrogeology and chemistry were introduced in solution mining, but they were confined to the study of permeability and granules properties [2,3]. With the continuous development of the computer software technology, fluid percolation in leaching dump has been gradually exposed by computational fluid dynamics method [4,5], but real seepage behaviors of the solution within the complicated granular media have not been effectively revealed. To fully understand the solution seepage process, accurate description of internal structure and detailed flow through the void space need to be resolved [6,7].

Magnetic resonance imaging (MRI), as one of the most advanced non-destructive detection technologies, has been widely used in medicine [8,9], chemical engineering [10,11] and other areas. Also, in dump leaching research, MRI can be used to investigate the porosity of granular media [12,13].

Therefore, in this study, to probe the structure and flow velocity within the interparticle space of a packed bed of agar beads under water-saturated condition, a laboratory experiment was carried out based on MRI technique. Images of the velocity field and internal structure of the bed were obtained. A study of pore structure and liquid flow velocity distribution in the porous media was performed by employing image

Foundation item: Project (51374035) supported by the National Natural Science Foundation of China; Project (2012BAB08B02) supported by the National Science & Technology Pillar Program During the Twelfth Five-year Plan Period; Project (NCET-13-0669) supported by the New Century Excellent Talents in University of Ministry of Education of China
Corresponding author: Sheng-hua YIN; Tel: +86-18811347208; E-mail: lchdaizi@163.com
DOI: 10.1016/S1003-6326(16)64208-5

processing technique. Based on the observed images of the porous media, the porosity and pore equivalent diameter of the sample were calculated. The velocity images at three different flow rates through the sample were obtained, and the quantitative flow velocity components of interstitial flow were determined from velocity maps by image analysis. Using this method, strong non-uniform flow fields were observed and the effect of flow rate on the velocity field was investigated. The MRI technique was introduced into the field of solution mining that make it feasible to study the seepage characteristics and evolution rules during heap leaching using non-contact and non-destructive detection technology.

2 Phase-contrast MRI for flow velocity measurement

Phase-contrast MRI (PC MRI) is a method that can measure the flow velocity based on phase change of magnetization vector caused by liquid flowing [14,15]. Under the dipolar magnetic field gradient, the phase change of protons has a linear relationship with the flow velocity. According to Hahn equation [16], the phase difference can be deduced as

$$\phi=\gamma m_i v_i \tag{1}$$

where ϕ is the phase change, γ is the gyromagnetic ratio, m_i is the initial magnetic field gradient, v_i is the pulse frequency. Through mathematics operation, Eq. (1) can also be expressed as

$$\frac{\mathrm{d}\phi}{\mathrm{d}G_i}=\gamma\Delta(\delta+t)v_i \tag{2}$$

where G_i is the pulsed field gradient, Δ is the pulse interval, δ is the pulse duration, t is the buffer time. By adjusting the gradient field, the velocity information of the flow can be obtained.

3 Experimental

3.1 Materials

In order to reduce the impact of metallic substance on imaging, spheroidal agar beads were used instead of mineral particles as the experiment material. To reduce the wall effect, the maximum grain size of the agar beads is about 12 mm that is one fifth of the inner diameter of the column.

3.2 Experimental apparatus

The apparatus is composed of a flow loop, an organic column and a MRI system, as demonstrated schematically in Fig. 1. The home-made multifunctional flow loop used for the whole experiment can conduct pore structure imaging experiment, column leaching experiment and seepage flow experiment for porous media. The volume flow rate through the column can be measured by a flowmeter and controlled artificially by the control valve. The internal diameter of the column is 60 mm with the maximum height of 220 mm.

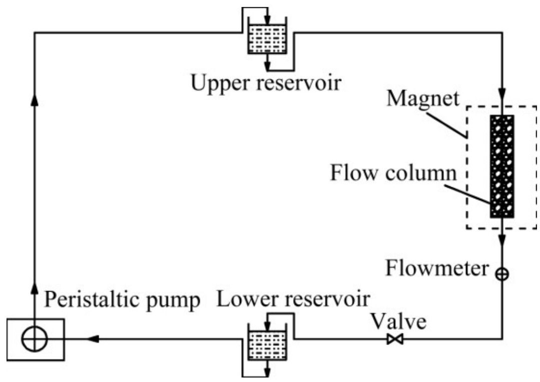

Fig. 1 Schematic drawing of flow loop

The type of MRI system is 3.0 T Discovery 750 (GE Medical System, US) with high performance whole-body gradients designed to deliver powerful amplitude of 50 mT/m and slew-rate of 200 T/(m·s) on each axis simultaneously, as shown in Fig. 2. FRFSE sequence and T1 FLAIR sequence were used in the MRI experiment. All images were acquired perpendicular to the axial plane with 4 mm in slice thickness, 0.4 mm in gap and 15 cm × 15 cm in field of view.

The acquisition parameters of the sequences are as follows (Fig. 3). FRFSE sequence: repetition time (TR)/echo time (TE) is 1000 ms/101.2 ms, and matrix size is 128×128 with the bandwidth of 90.9 kHz. T1 FLAIR sequence: repetition time (TR)/echo time (TE)/inversion time (TI) is 1814 ms/28.5 ms/750 ms with the bandwidth of 31.2 kHz.

3.3 Experimental procedure

Firstly, to maintain the experimental materials under water-saturated condition, the column was filled with water and the agar beads were immersed in water. After ensuring that all surfaces were free of air bubbles, the spheres were poured into the column and the top portion of the column was fitted to form a seal to prevent air from entering the system [17]. At this point, all of the void spaces in the porous media were occupied by water.

Secondly, to obtain a constant flow rate through the column, the control valve was regulated and the water was pumped from the lower reservoir to the upper reservoir by variable speed peristaltic pump. The measurements of the flow rate were repeated several times during the experiment to ascertain the flow rate and ensure that it was stable over time [18].

Finally, after putting the column into the MRI

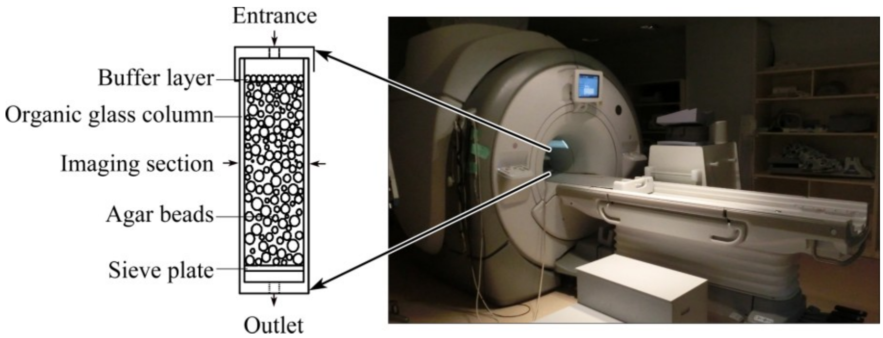

Fig. 2 MRI experiment system

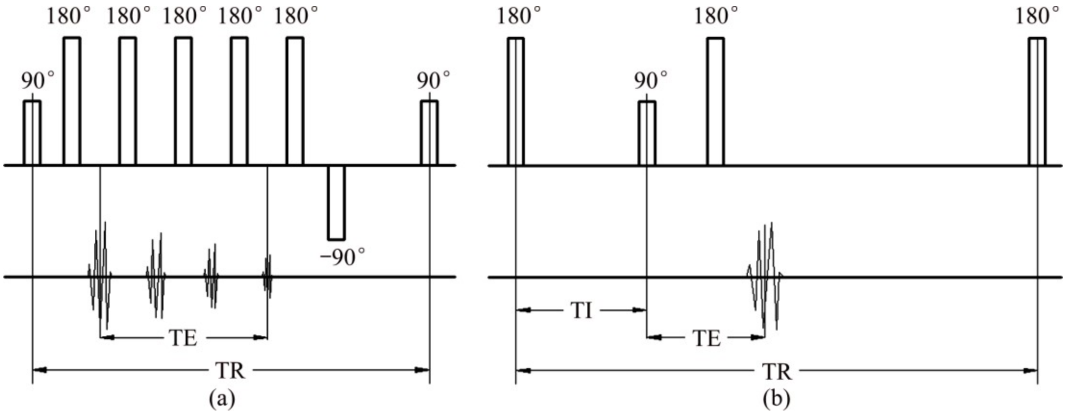

Fig. 3 Sequences used in MRI experiment: (a) FRFSE sequence; (b) T1 FLAIR sequence

machine, the fluid was passed in the continuous loop through the magnet. Flow visualization was achieved using the T1 FLAIR sequences and the velocity images within the porous media were obtained. By regulating the control valve, the authors find that the maximum flow rate through the column is about 0.6 L/min. The MRI experiments were conducted at the flow rates of 0.3, 0.4 and 0.5 L/min, respectively.

When the macroscopic flow yielded a value of 0, it means that the water in the column was perfectly still. In the similar way, the internal pore structure images of the porous media were obtained in the absence of flow but with the void space filled with water.

4 Results and discussion

4.1 porosity

Figure 4(a) shows an MRI image of a cross-section of the column, which demonstrates the tomographic cut through the column packed with agar beads perpendicular to its axis. The black areas in the image correspond to the beads and the white areas correspond to the water that fills the pore space [19]. In order to calculate the porosity of the porous media, it is highly indispensable to pre-process the original MRI images. To know clearly the boundary between particles and pores, the thresholding and boundary extracting technique was applied, as shown in Fig. 4. The extent of regions of pores and their connectivity are characterized by identifying percolating paths of water. It can be seen from Fig. 4(b) that the porosity is the ratio of pore area to the whole image area. Namely, it is the ratio of pixel number of white area to the total pixel number in the column.

After per-processing, the area occupied by each pore can be obtained from Fig. 4(c). Therefore, the porosity ϕ can be demonstrated as

$$\phi = \sum_{i=1}^{n} a_i / A \tag{3}$$

where A is the cross-section area of the column, i is the serial number of the pore, a_i is the area of pore i, n is the number of the pores. According to Eq. (3), the porosity of the porous media is 31.28% by computing the mean of porosities of all the cross-sections.

4.2 Pore equivalent diameter

After getting the area of every pore on the cross-section, the pore equivalent radius can be calculated as

$$R_i = \sqrt{a_i / \pi} \tag{4}$$

where R_i is the equivalent radius of pore i. Based on statistical method, the distribution of pore equivalent diameter within the porous media is acquired, as shown

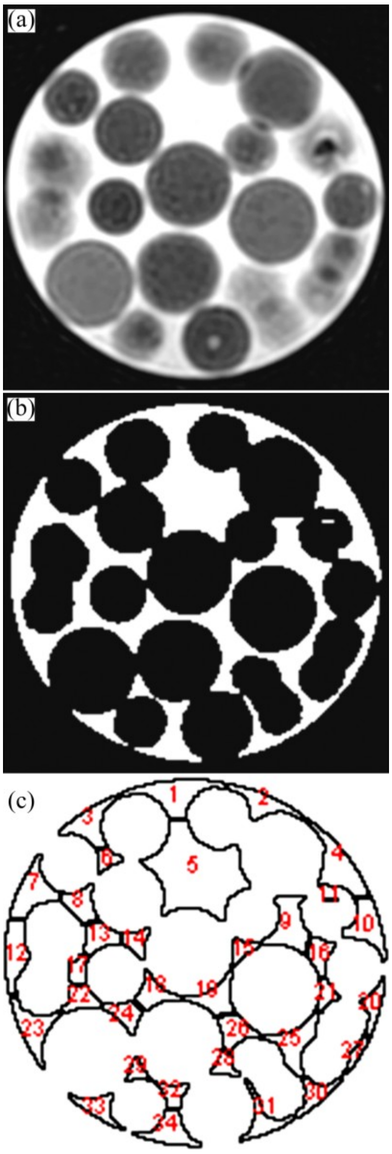

Fig. 4 Preprocessing procedure of MRI images: (a) Original image (solid matrix is shown as black and liquid as white); (b) Binary pore image (pore is white); (c) Pore boundary image

in Fig. 5. Most of the pore equivalent diameters concentrate in 2.0−3.5 mm, and the maximum value is 7.1 mm, which belongs to pore 5 in Fig. 4(c). The fitting curve for the distribution of pore equivalent diameter follows Gaussian distribution (Expected value μ=2.48, standard deviation σ=0.99).

The result manifests that the pore-parameter measurement by MRI can provide not only bulk property but also local properties. The inner structural parameters and the correlation between the pores can be investigated based on the obtained porosity and pore equivalent diameter. Furthermore, the image analysis based on MRI technology would have the advantage of determining the pore distribution and network structure to characterize the interstitial flow through the porous media [20].

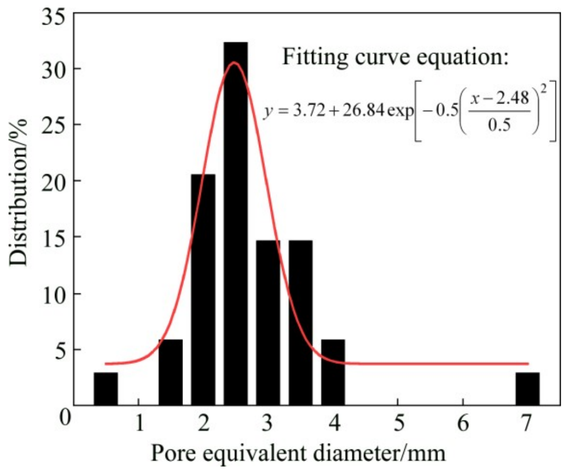

Fig. 5 Distribution of pore equivalent diameter (Solid line is fitting curve)

4.3 Flow velocity field

The velocity images in the same slice at three different flow rates are shown in Fig. 6, and the measurements were carried out for a single-phase flow of water. In Fig. 6, the area with whiter color corresponds to higher flow velocity. Obviously, the local velocity profiles are affected greatly by flow rate. The higher the flow rate is, the lighter the image is.

In order to study the liquid velocity distribution, the quantitative flow velocity maps were created using image processing technique, as shown in Fig. 7. To compare flow rates calculated with flow rates measured at the flowmeter, the sum of the velocity components in each pore was figured out. The result demonstrates that the flow rate calculated from velocity images just has error less than 8% with the corresponding experimental value.

The velocity maps in Fig. 7 show that the water flow through the void space is not a homogeneous flow in any pores. Since the non-uniform flow strongly affects the dispersive phenomenon in the porous media, it is necessary to get the local flow velocities in the pores and extract the characteristics of interstitial flow depending on the complex pore structure.

4.4 Effect of flow rate on velocity field

The velocity data from pores, marked with squares A−F in Fig. 7, are shown in Fig. 8. In these plots, the way that the velocity depends on the flow rate is demonstrated at the flow rates of 0.3, 0.4 and 0.5 L/min. As shown in Fig. 8, the contour lines do shift in the pore as the flow rate varies, which is clearly manifested by the contours. It is also clearly demonstrated that the velocity distributions within the pore are roughly parabolic, with the local maximum being near the center and the

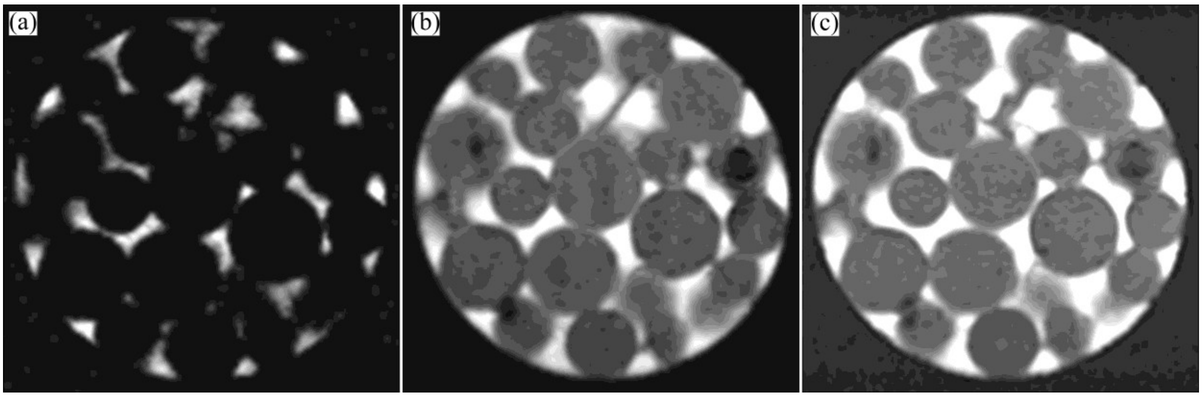

Fig. 6 Liquid velocity images at three different flow rates: (a) 0.3 L/min; (b) 0.4 L/min; (c) 0.5 L/min (Lighter shades indicate higher velocities)

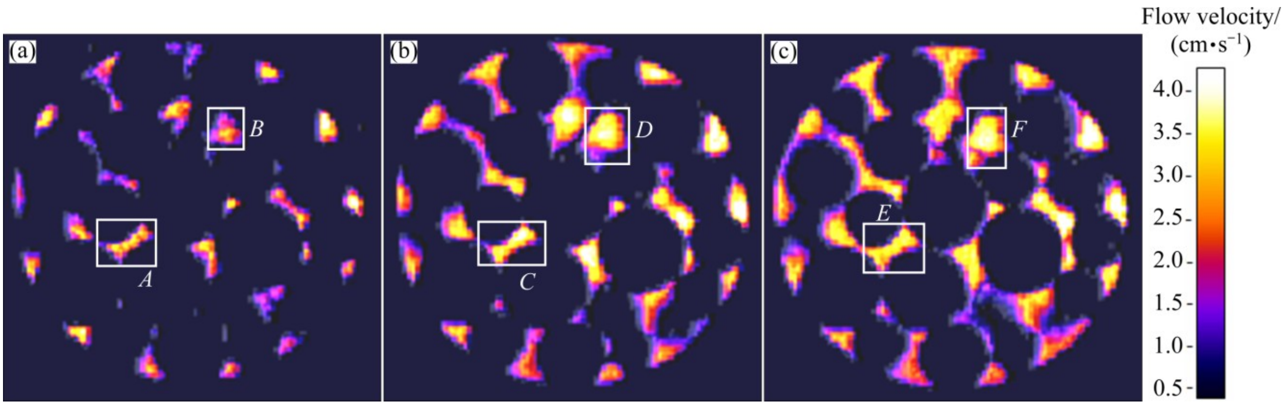

Fig. 7 Quantitative velocity maps of water flow though packing agar bead at three different flow rates: (a) 0.3 L/min; (b) 0.4 L/min; (c) 0.5 L/min (Marked pores are enlarged in Fig. 8)

velocity decreasing to the wall of the pore. The result coincides with the NMR imaging of flow in the bead packs used by KUTSOVSKY et al [19], but contrasts with the conclusions obtained by NESBITT et al [21]. It may be caused by the fact that the experiment materials used in this experiment do no correspond with the materials selected by NESBITT et al [21].

In order to study the statistical characterization of the flow velocity, the frequency distribution of the normalized velocity was obtained from the velocity images in the same slice in Fig. 6 at three different flow rates, as shown in Fig. 9. The statistical distribution has been determined from the velocity components with over 6000 data points, and the frequency as the ordinate has been normalized by the number of components [20].

Figure 9 shows that half of the velocity components are in the class of 0−1 cm/s. Although the frequency of higher velocity rapidly decreases, the values exceeding 4 cm/s are still observed. It is interesting to note that the frequency of lower velocity components is higher at lower flow rate, but to higher velocity components, it is just the opposite, as can be seen in Fig. 9.

5 Conclusions

1) Based on image pre-processing, the porosity and pore equivalent diameters of the porous media were determined. The porosity of the sample is 31.28% by calculation and the fitting curve for the distribution of pore equivalent diameter conforms to the law of Gaussian distribution (μ=2.48, σ=0.99).

2) The quantitative flow velocity maps were created using image processing. It demonstrates that the interstitial flow through the packed bead is not a homogeneous flow in any pores.

3) The contour plots show that the flow velocities do shift in the pore as the flow rate varies. Furthermore, the velocity distributions within the pores are roughly parabolic, with the local maximum being near the center and the velocity decreasing to the wall of the pore.

4) The frequency distributions of the velocity components of flow through the void space were created using the method of mathematical statistics. It is shown

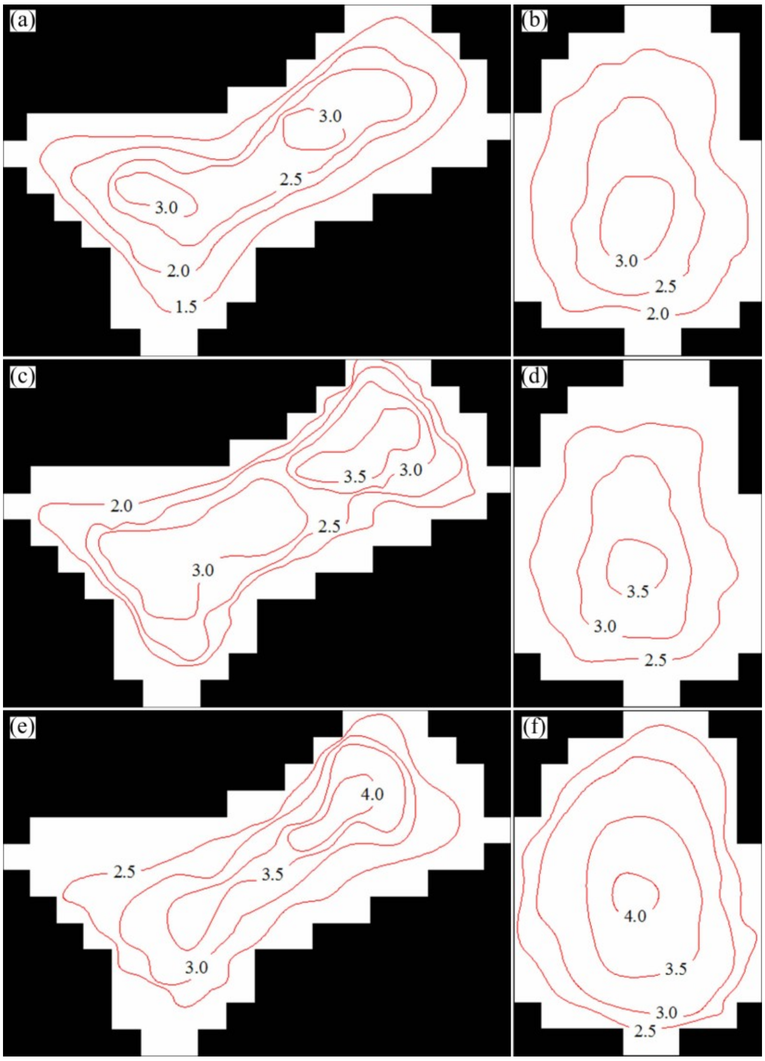

Fig. 8 Contour plots (a)−(f) of velocity in pores marked with squares *A*−*F* in Fig. 7, respectively (unit: cm/s)

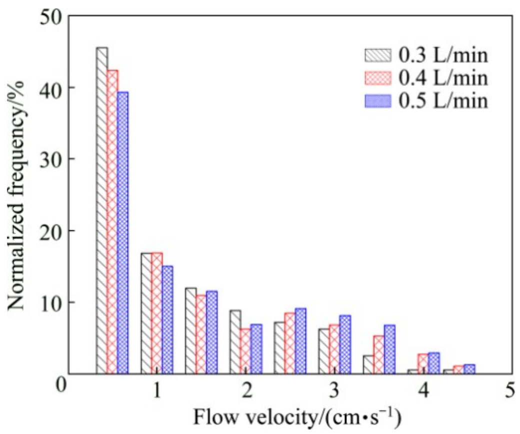

Fig. 9 Frequency distributions of normalized velocity components of interstitial flow through packed agar beads at three different flow rates

that half of the velocity components are in the class of 0−1 cm/s. The frequency of lower velocity components is lower at higher flow rate, but to higher velocity components, it is just the opposite.

References

[1] JOEKAR-NIASAR V, DOSTER F, ARMSTRONG R T, WILDENSCHILD D, CELIA M A. Trapping and hysteresis in two-phase flow in porous media: A pore-network study [J]. Water Resources Research, 2013, 49(7): 4244−4256.

[2] MANFRED K, LAURA B, MATTHIAS B, JOHANNES I. Nitrate leaching is not controlled by the slurry application technique in productive grassland on organic-sandy soil [J]. Agronomy for Sustainable Development, 2014, 35(1): 1−11.

[3] MIAO X, WU A, YANG B, LIU J, YIN S, WANG H. Unsaturated flow and solute transport in a porous column using spherical ore particles [J]. International Journal of Minerals Metallurgy & Materials, 2014, 21(2): 113−121.

[4] CARIAGA E, CONCHA F, SEPÚLVEDA M. Flow through porous media with applications to heap leaching of copper ores [J]. Chemical Engineering Journal, 2005, 111(2): 151−165.

[5] BOUFFARD S C, RIVERA-VASQUEZ B F, DIXON D G. Leaching kinetics and stoichiometry of pyrite oxidation from a pyrite-marcasite concentrate in acid ferric sulfate media [J]. Hydrometallurgy, 2006, 84(3−4): 225−238.

[6] YANG Bao-hua, WU Ai-xiang, YIN Sheng-hua. Simulation of pore

scale fluid flow of granular ore media in heap leaching based on realistic model [J]. Journal of Central South University of Technology, 2011, 18(3): 848−853.
[7] STEWART M L, WARD A L, RECTOR D R. A study of pore geometry effects on anisotropy in hydraulic permeability using the lattice-Boltzmann method [J]. Advances in Water Resources, 2006, 29(9): 1328−1340.
[8] LAI H Y, YOUNCE J R, ALBAUGH D L, SHIH Y Y. Functional MRI reveals frequency-dependent responses during deep brain stimulation at the subthalamic nucleus or internal globus pallidus [J]. Neuroimage, 2014, 84(1): 11−18.
[9] MELLERIO C, LABEYRIE M, CHASSOUX F, ROCA P, ALAMI O, PLAT M, NAGGARA O, DEVAUX B, MEDER J, OPPENHEIM C. 3T MRI improves the detection of transmantle sign in type 2 focal cortical dysplasia [J]. Epilepsia, 2014, 55(1): 117−122.
[10] ZIVADINOV R, TREU C N WEINSTOCK-GUTTMAN B, TURNER C, BERGSLAND N, O'CONNOR K, DWYER M G, CARL E, RAMASAMY D P, QU J, RAMANATHAN M. Interdependence and contributions of sun exposure and vitamin D to MRI measures in multiple sclerosis [J]. Journal of Neurology Neurosurgery & Psychiatry, 2013, 84(10): 1075−1081.
[11] CALAMANTE F. Arterial input function in perfusion MRI: A comprehensive review [J]. Progress in Nuclear Magnetic Resonance Spectroscopy, 2013, 74(10): 1−32.
[12] NGUYEN N L, VAN B V, REIMERT R, VON G A. Determination of porosity and flow distribution in packed beds by magnetic resonance imaging [J]. Magnetic Resonance Imaging, 2005, 23(2): 395−396.
[13] SANKEY M H, HOLLAND D J, SEDERMAN A J, GLADDEN L F. Magnetic resonance velocity imaging of liquid and gas two-phase flow in packed beds [J]. Journal of Magnetic Resonance, 2009, 196(2): 142−148.
[14] WU Ai-xiang, XUE Zhen-lin, YIN Sheng-hua, WANG Heng. Study of the granular medium structure of mine rock and solution distribution based on MRI technology [J]. Journal of China University of Mining & Technology, 2014, 43(4): 582−587. (in Chinese)
[15] YIN Sheng-hua, XUE Zhen-lin, WU Ai-xiang, LIU Chao, LI Hong. Mesoscopic seepage velocity characteristics during heap leaching based on magnetic resonance imaging [J]. Chinese Journal of Engineering, 2015, 37(3): 275−280. (in Chinese)
[16] ATAKISHIYEV N M, SUSLOV S K. The Hahn and Meixner polynomials of an imaginary argument and some of their applications [J]. Journal of Physics A: Mathematical and General, 1985, 18(10): 1583−1596.
[17] SEDERMAN A J, JOHNS M L, BRAMLEY A S, ALEXANDER P, GLADDEN L F. Magnetic resonance imaging of liquid flow and pore structure within packed beds [J]. Chemical Engineering Science, 1997, 52(14): 2239−2250.
[18] SEDERMAN A J, HOHNS M L, ALEXANDER P A, GLADDEN L F. Visualisation of structure and flow in packed beds [J]. Magnetic Resonance Imaging, 1998, 16(5−6): 497−500.
[19] KUTSOVSKY Y E, SCRIVEN L E, DAVIS H T, HAMMER B E. NMR imaging of velocity profiles and velocity distributions in bead packs [J]. Physics of Fluids, 1996, 8(4): 863−871.
[20] OGAWA K, MATSUKA T, HIRAI S, OKAZAKI K. Three-dimensional velocity measurement of complex interstitial flows through water-saturated porous media by the tagging method in the MRI technique [J]. Measurement Science & Technology, 2001, 12(2): 172−180.
[21] NESBITT G J, GROOT A D, FENS T W, BONNIE J H M. Towards validation of porous media models using NMR imaging and image-analysis techniques [J]. Magnetic Resonance Imaging, 1991, 9(5): 779−787.

基于核磁共振成像技术的饱和多孔介质孔隙结构及溶液流速分布探测

吴爱祥 [1,2]，刘 超 [1,2]，尹升华 [1,2]，薛振林 [1,2]，陈 勋 [1,2]

1. 北京科技大学 金属矿山高效开采与安全教育部重点实验室，北京 100083；
2. 北京科技大学 土木与环境工程学院，北京 100083

摘　要：为了探测多孔介质的内部结构及颗粒间流速分布，对饱和条件下的琼脂球散体进行核磁共振成像试验，获取了 3 种流量下的速度场图像。同时，为了确定多孔介质的孔隙参数，利用图像处理技术获取了其内部结构。结果表明：该多孔介质的孔隙率为 31.28%，其孔隙当量直径分布拟合曲线满足高斯分布；流速场随着流量的改变而变化且孔隙内的流体为非均质流；孔内流速分布近似于抛物线状，局部最大值位于中心附近；约一半的速度分量在 0~1 cm/s 之间；流量越大，低速度分量的频率越低，而对于高速度分量，则恰恰相反。

关键词：核磁共振成像；多孔介质；流速；孔隙率；孔隙当量直径

(Edited by Mu-lan QIN)